Boundary-layer oscillations from thunderstorms at Sydney Airport

Richard Manasseh and Jason H. Middleton
School of Mathematics, University of New South Wales
Sydney, Australia

Abstract

Analyses of wind velocity and air pressure data, acquired by a set of low-level anemometers at Sydney Airport, Australia, indicate the passage of a set of three remarkably smooth atmospheric boundary-layer oscillations that travelled ahead of a thunderstorm on 27 December 1991. The oscillations were probably generated by a nearby thunderstorm outflow, propagating into a stably stratified atmospheric layer. It is likely that the phenomenon was initiated by the degeneration of an outflow gravity current into a family of amplitude-ordered solitary waves. Although reasonable agreement can be obtained on the propagation speed using a linear theory, the weakness of the trapping mechanism for this solution and an over-estimation of the weakly nonlinear wave half-width leads to a conclusion that the waves were fully nonlinear.

1 Introduction

There are two aims of a currently ongoing study of low-level wind shear at Sydney Airport, using data recorded on a continuous basis since mid 1991. The immediate aim is an analysis of the fluid-dynamical behaviour during strong low-level wind shear episodes, with an emphasis on thunderstorm-generated phenomena. The long-term goal is the generation of statistics on the occurrence of severe horizontal wind shear in the Sydney Airport region, since wind shear is a hazard to aircraft. (The US Low-Level Wind Shear Alert System alarm threshold is equivalent to a difference of about 7.7 m s^{-1} over 2.8 km.) Thunderstorms are recognized as a source of wind shear that may be particularly dangerous when aircraft are landing or taking off (Fujita and Caracena 1977).

Several studies (e.g. Mahoney and Elmore 1991; Lee et al 1992a, 1992b) have focussed on the thunderstorm-generated microburst phenomenon, which has been associated with a number of aircraft accidents. However, the present observations, which were made during the 1991/92 Sydney summer thunderstorm season, indicate that unexpected low-level wind shear at this location can also be caused by atmospheric waves. A common pre-requisite for long wave propagation, either linear waves or nonlinear solitary waves, is the existence of a stably stratified layer, which, together with an appropriately sheared atmosphere, can act as a waveguide. Linear long-wave energy, if trapped in a waveguide, could propagate considerable distances from a disturbance source. A stably stratified layer may also be a waveguide (Benjamin 1967; Davis and Acrivos 1967) suitable for the propagation of nonlinear solitary waves.

Balachandran (1980) described observations of both long-period waves (3 h) and short-period waves (down to 290 s) generated by thunderstorms in the northeastern United States. Wave trapping in a waveguide where a critical layer was present at the tropopause permitted propagation of the oscillations over 1000 km, with "remarkable stability in the shape and amplitude of the waveform". Shear instabilities of thunderstorm outflows were identified as the most likely source of the waves but Balachandran did not speculate further on the details of the wave-generating mechanism. It was proposed that the waves in turn generated other thunderstorms by uplifting conditionally unstable air.

Fulton et al (1990) analysed a phenomenon recorded by an instrumented tower at Norman, Oklahoma, United States. Although the surface data had some features of a 'classic' thunderstorm cold outflow, there were some unusual features, in particular three periodic wind surges that were later observed to propagate for several hours. They interpreted the observations to include a "bore-like wave initiated by the cold outflow, ... moving at a speed which is overtaking the outflow current." Fulton et al were able to roughly estimate the speed of propagation that a gravity current would have to have, given the temperature profile observed by their instrumented tower; the resulting estimate was far too low, rendering a gravity current an improbable explanation. Their conclusion was that the phenomenon was a thunderstorm-generated gravity current degenerating into a family of solitary waves. Shreffler and Binkowski (1981) had suggested that propagating pressure jump lines observed in the United States (which may represent solitary waves) were caused by thunderstorm outflows impacting a temperature inversion. Laboratory realizations of the scenario in which gravity currents engender solitary waves are given by the experiments of Rottman and Simpson (1989). Laboratory thermals hitting a density interface – a situation which may model thunderstorm events – were shown to generate solitary waves by Noh et al (1992). Fulton et al (1990) also present a reexamination of some previous observations of boundary-layer oscillations in the light of the solitary wave scenario.

A thunderstorm-generated solitary gust was identified by Doviak and Ge (1984) in Oklahoma, United States, and a solitary-wave theory developed by Doviak et al. (1991) was subsequently applied to that event. The theory is based on a solution to a form of the Benjamin-Davis-Ono equation, which was modified for vertical shear and compressibility. It shows fair agreement with observations in general, although the wave speed is significantly overestimated, probably because of the breakdown of the weakly nonlinear hypothesis (Doviak et al 1991).

Several observations of atmospheric solitary waves that are generated by large scale processes have been made. Some of these are typified by the 'Morning Glory' of northern Australia that is associated with mesoscale phenomena. (For example, Clarke et al 1981; Haase and Smith 1984; Christie 1992.) Examples of weakly nonlinear calculations made to try to explain these phenomena are found in Noonan and Smith (1985) and Rottman and Einaudi (1993). The latter work achieves good agreement with a morning glory previously analysed by Noonan and Smith (1985) although Rottman and Einaudi noted that in order to do so, a wave amplitude had to be chosen that probably rendered the weak nonlinear assumption invalid, making their result possibly fortuitous. They also analysed a synoptic-scale thunderstorm-generated wave, achieving good agreement if the trapping height was chosen at the altitude of a critical layer. A train of solitary waves observed by Physick (1986) was associated with a synoptic-scale trough. Morning-glory-like waves reported by Smith (1986) are thought to have been generated by the interaction of a thunderstorm gust front with a sea-breeze front. On a smaller scale, while several instrumented observations of thunderstorm outflows have been made (Simpson 1987), descriptions of small-scale boundary-layer atmospheric waves that are thunderstorm-generated seem limited to those of Doviak and Ge (1984) and Fulton et al (1990).

2 Observations

Sydney Airport is sited on a coastal plain in the eastern metropolitan area of Sydney. The instrumentation at Sydney Airport (figure 1) consists of five tower-mounted anemometers on the airfield plus a sixth at Kurnell. The anemometers are about 13 m above ground level (and thus, effectively 'at sea level') and well sited away from obstructions, with the exception of sensor 6, which suffers from a higher wind variance owing to its proximity to a sand dune. The wind speeds and directions and are logged every two seconds at each sensor. Air pressure at the airport's meteorological station is also logged, at ten-second intervals. The data is transmitted in real time to the University of New South Wales (UNSW) for daily analysis and archiving. The staff at the airport's meteorological station record observations every half hour and more frequently during unusual conditions. A weather radar located at the airport identifies precipitation zones on the basis of their radar reflectivity. The radar's associated software automatically tracks storm centres in order to warn aircraft of their development. The meteorological station also makes regular radiosonde measurements, subject to aircraft movements.

The period of interest is from 2135 Eastern Daylight Saving Time (EDT) on 27 December 1991 to about 0020 EDT on 28 December. (EDT = Universal Time + 11 h, and all subsequent times quoted herein will be in EDT.) The day was clear and warm, with a maximum surface temperature of 28°C occurring at 1430. Radiosonde measurements (described in detail in §3) indicated that a temperature inversion, present since the previous day, had persisted up to the last sounding (at 1500) before the event occurred. The inversion was due to a layer of air about 3° cooler than the ground temperature, which existed up to about 570 m above ground level (AGL). The ground temperature was 27°C at the time of the sounding and fell as the afternoon and evening progressed; it was 23°C by 2000. An extrapolation to ground level along a dry adiabat of the upper-level temperature profile (close to dry adiabatic) indicates a temperature around 35°C if the inversion were absent. Since the sounding was made at the coast, the possibility that the inversion was a purely maritime effect should be considered. The prevailing winds were approximately parallel to the coast throughout the morning. Observations from nine sites will be used to determine the propagation velocity of the phenomenon about to be described. Of these, seven were on the coast, or out to sea. Thus it is reasonable to presume that the inversion was also present at

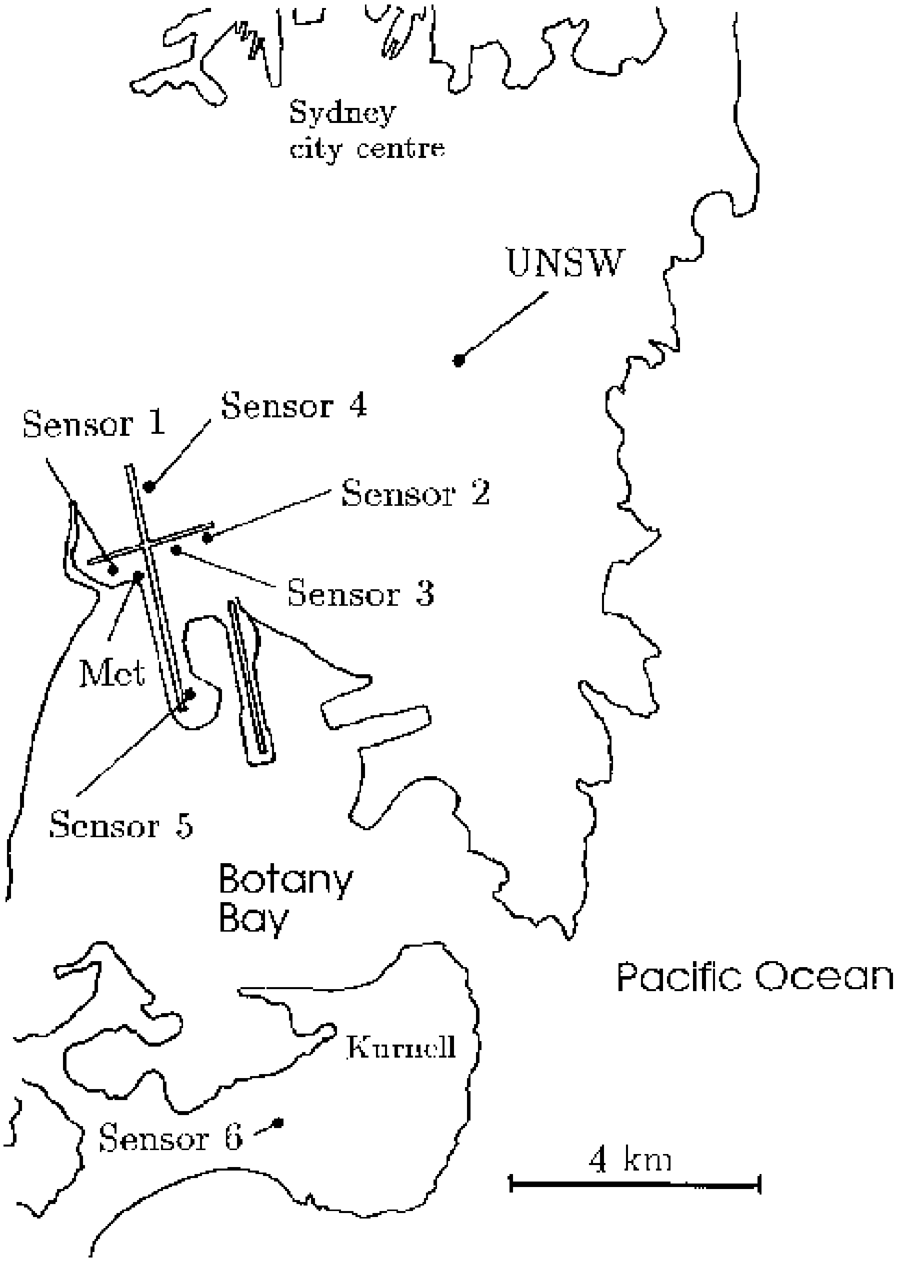

Figure 1: Sensors 1 to 5 are on the Sydney Airport airfield: Sensor 1 and Sensor 2 are at the ends of the shorter runway. Sensor 4 and Sensor 5 are at the ends of the longer runway. Sensor 6 is at Kurnell and is currently of limited use owing to poor siting. Met: the airport's meteorological station.

those sites. At Bankstown, 18 km inland, the ground-level temperature at 1500 was 29°C, still somewhat less than the estimate of 35°C if the inversion were absent.

At the airport sounding site, the warm surface air, in the first 150-200 m AGL, was statically unstable and would have been warming the inversion throughout the afternoon. The ground-level relative humidity at 2000 was about 82%.

These are typical germinal conditions for summertime thunderstorms in this area. Radar pictures prior to 2130 (see, for example, Figure 2) show a large area of cloud over 50-120 km to the south and southwest of Sydney Airport. This is a region of escarpments to over 400 m that is relatively hilly compared with the Sydney basin; it is often the location of convective activity. At 2000 a thunderstorm was identified with its centre (defined as a zone of rainfall over 27 mm per hour) on a bearing of 233° from the airport and 110 km away. The storm centre moved radially towards the airport over the next few hours at speed of roughly 40 km per hour. At 2130 the storm centre was about 65 km away on the same bearing. From 2000 to 2130, there were five brief (i.e. apparent over a single 3-minute radar sample period) occurrences of small zones of heavy rainfall with precipitation rates greater than 48.6 mm per hour. Four of these zones were at the first storm centre and a fifth was at a secondary storm centre about 55 km north-west of the first centre.

From the airport's meteorological station, low clouds were not visually apparent until 2100, when one octa of cumulonimbus could be seen. Lightning was noted to the south-west of the airport. The wind at the airport was north-north-easterly at 8 m s^{-1}.

a. *Undular changes in wind velocity*

At the airport at 2135 there was a sudden change in the wind direction to south-westerly. Clear conditions were still being reported over the airport - there was no precipitation or low cloud. The change arrived first at sensor 6 (at Kurnell, 7.5 km south-east of the airport), then at the airport, at sensors 1 and 5, then sensor 3 and finally sensors 2 and 4, indicating that it was propagating from the south-west to the north-east. It crossed the airfield in 2 minutes ±30 s, and was recorded 20 minutes later at the Ocean Reference Station (ORS1) (located about 13 km east-north-east of the airport). The

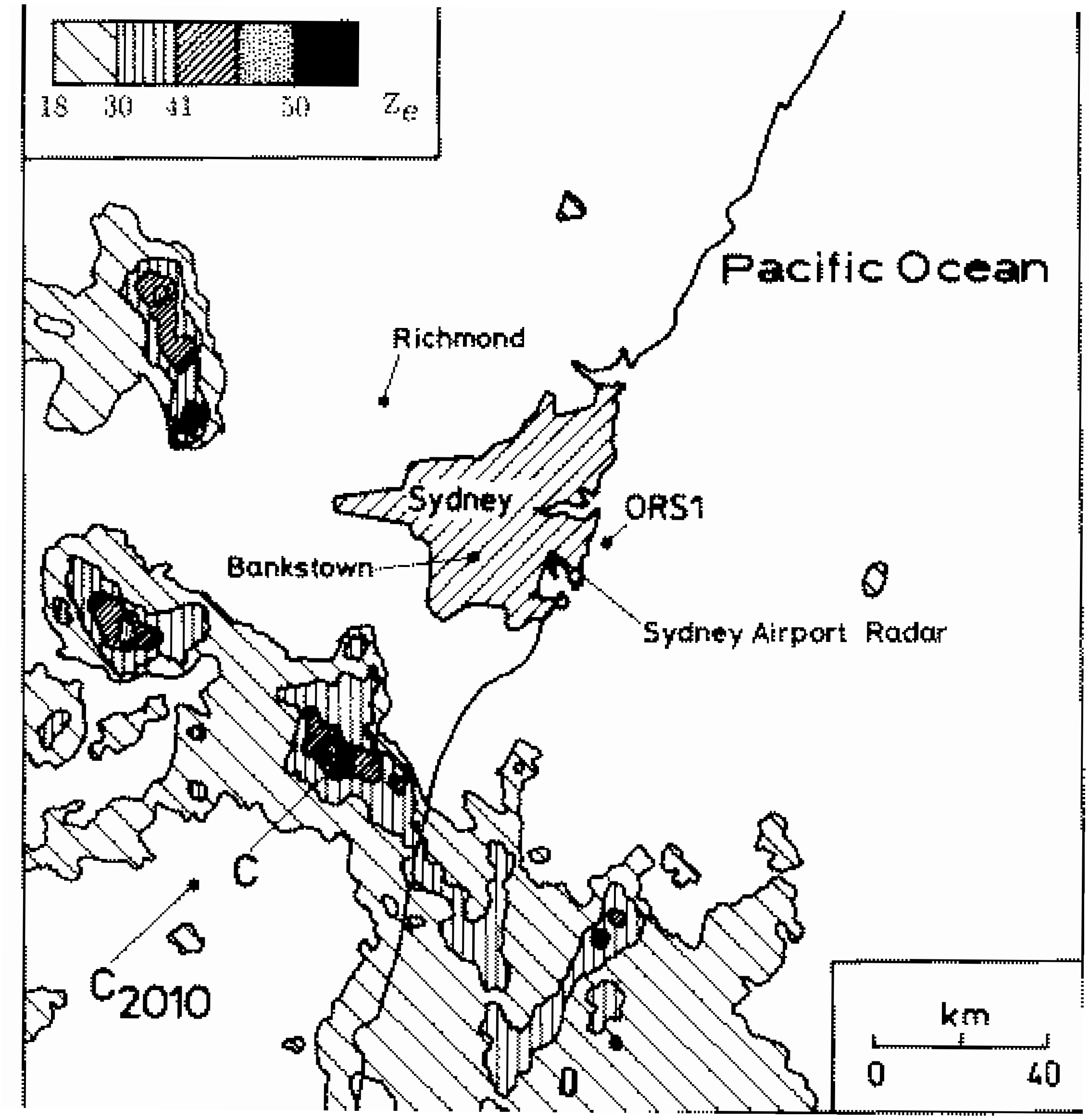

Figure 2: Weather radar picture for 2118 to 2121, 27 December 1991. Contours are of effective reflectivity factor (Z_e). There is a single zone of $Z_e \geq 50$ dBZ (48.6 mm hour^{-1}) which is marked 'C'; this corresponds to the original storm centre which was moving towards the airport at roughly 40 km hour^{-1}. The position of the storm centre at 2010 is marked 'C_{2010}'. The radar makes three scans at elevations of 1.5°, 3.0° and 4.5° which are combined by a range-dependent formula; the highest reflectivity zone 'C' is sectioned at about 3500 m above sea level (3100-3300 m AGL).

timeseries of wind vectors on Figure 3 show the wind speed increase to a peak, then fall off to calm conditions, then rise and fall twice more, in an undular fashion. The wind records in Figure 3 are the raw data with every two-second sample shown, without filtering or smoothing. The net change in wind speed from before the event to the peak can be roughly estimated at 17 ± 5 m s^{-1}.

The pressure record (in raw form) shows a co-incident set of undulations. The maximum pressure rise to the peak of the first undulation is roughly 3 mbar; Christie (1992) describes morning glory waves with the equivalent rises being about 1 mbar. The temperature record also showed similar undulations. (The temperature resolution of the temperature record, based on an analogue pen recorder, is poorer than the pressure resolution of the presure record.) There was no net change in temperature after the passage of the three undulations. The wind velocity and pressure records show that the half-height of the peak-to-trough speed undulations decreased progressively, from about 7 m s^{-1} in the first to about 4 m s^{-1} in the third. The record at ORS1 (Figure 4, which is also in an unfiltered form) has samples only every 30 seconds and is less smooth, perhaps owing to the motion of the buoy on which its anemometers are mounted, only 4.5 and 5 m above sea level; it shows the first south-westerly change clearly and also the second and third undulations, albeit less smoothly.

A record of the undulations is also available from Bankstown, which is about 18 km west of Sydney Airport and at effectively the same elevation. The Bankstown record (Figure 5) shows four clear oscillations in wind direction and possibly a fifth. The peak direction of the first directional oscillation was west-south-westerly, the second southerly and the following three changing slightly in direction towards the easterly with the putative fifth representing winds from 160°. The initial change at Bankstown (defined as the time when the wind turned through due easterly) occurred at about 2125. At Bankstown there were no prevailing winds in the hour before the phenomenon. The peak wind speed change (8 m s^{-1}) was lower than at Sydney Airport. At Lidcombe, 14 km north-west of Sydney Airport, another anemometer provided lower-resolution data. Its record is similar to that at Bankstown, with four clear directional oscillations. The peak wind speed change here was about 6 m s^{-1}.

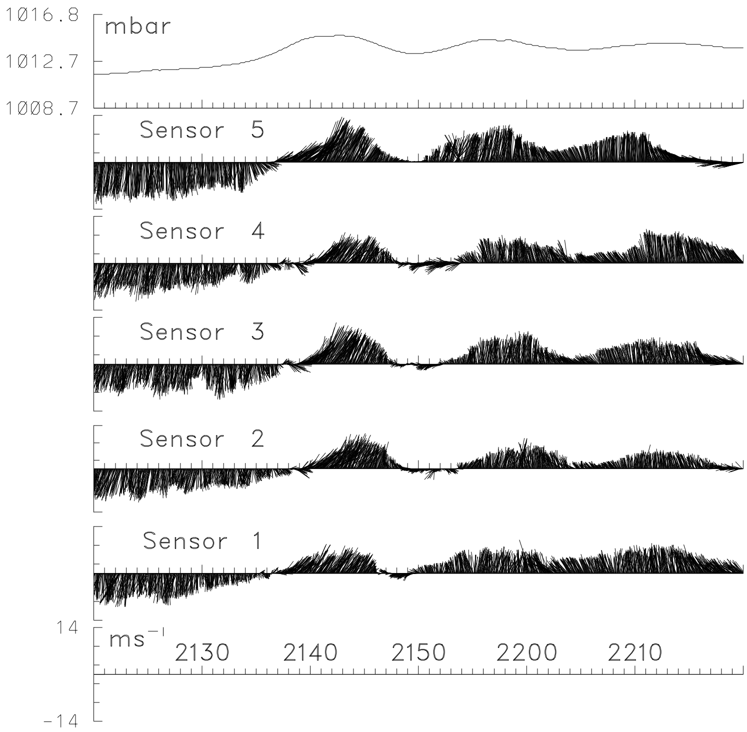

Figure 3: The event arriving at Sydney Airport, 27 December 1991. Wind vectors point in the direction to which the wind is blowing; their length indicates the wind speed. Time in minutes runs along the bottom axis, where zero corresponds to 2120.

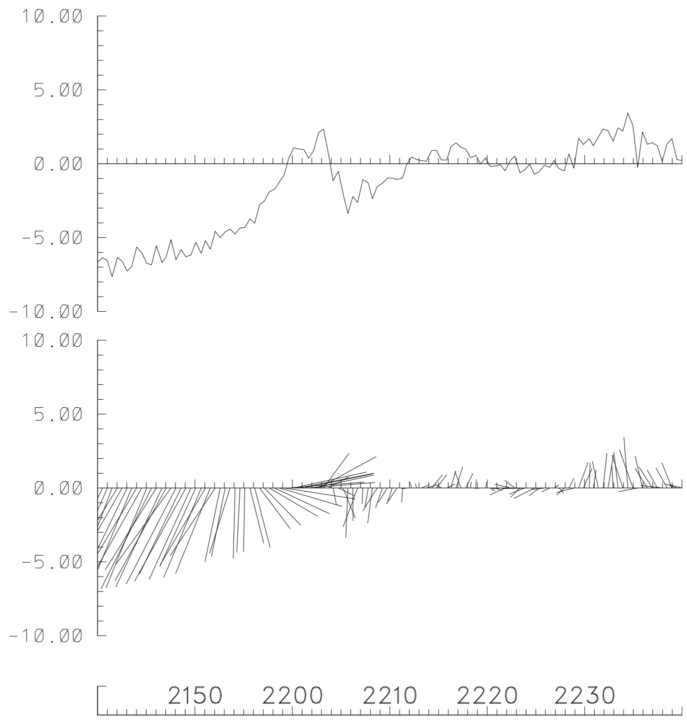

Figure 4: The event arriving at the Ocean Reference Station (ORS1) on 27 December 1991. Wind vectors point in the direction to which the wind is blowing; their length indicates the wind speed. In order to better delineate the event, the upper graph shows the component of wind velocity along the north-south line, with positive meaning a southerly wind. (A second, redundant anemometer provided virtually identical data.)

Figure 5: The event arriving at Bankstown, 27 December 1991.

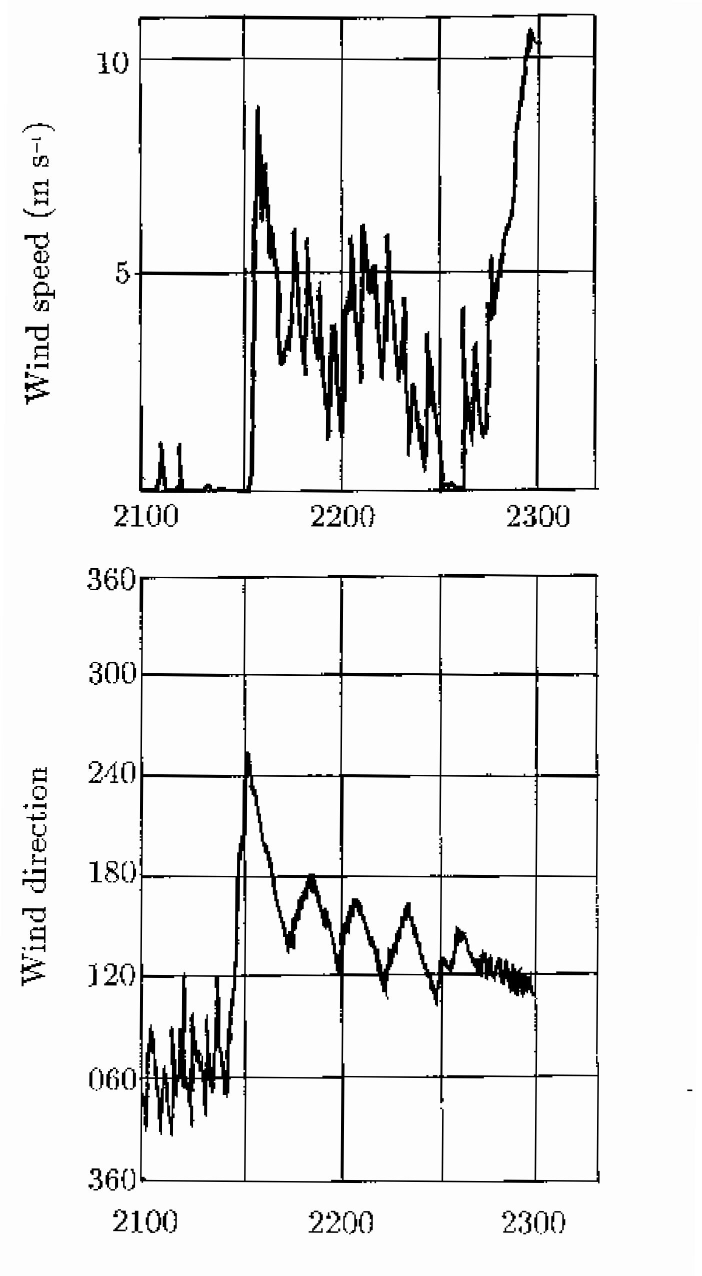

b. Subsequent events

At an anemometer at Richmond, about 57 km north-west of Sydney Airport, there is no evidence of an undular phenomenon, though there is a sudden gust to 7 m s^{-1} and wind change from easterly to south-westerly at 2145. It is possible, however, that this was associated was a local thunderstorm cell 10 km south-west of Richmond that generated heavy (greater than 48.6 mm per hour) rainfall zones at 2136.

Following the undulations at the airport, the wind had become temporarily calm by about 2235. At 2230 thunderstorm conditions were reported over the airport, reaching the 'mature' stage around 2400, when there were 5 octas of cumulonimbus. A south-easterly wind of about 5-7 m s^{-1} was blowing during most of this time and the pressure was steady. However, in the 14 minutes from 2334 to 2348 there was a rapid pressure change: a 2 mbar rise, then a 4 mbar drop that was accompanied by an abrupt change in the wind direction to easterly. This easterly change propagated across the airfield in 2 minutes ± 30 s. The wind following it was about 12-15 m s^{-1}. Although it travelled from the south-east to the north-west across the airport, easterly winds did not arrive at Kurnell, to the south east, until the change was already at the airport, indicating that it was an event with a complex frontal structure on the local scale (5-10 km). Meanwhile, the temperature dropped from 21.4°C at 2356 to 18.2°C at 0004, then increased to 19.7°C at 0020. From 2400 to 0015 a further change in wind direction, to north-easterly, propagated across the airfield. By 0030 the cumulonimbus had dissipated. The wind remained north-easterly until 0130, when it changed to northerly, remaining that way for the next three hours.

c. Speed of travel of the phenomenon

The undular phenomenon that occurred from 2135 to about 2235 will be called *Event 1* – it is the subject of this paper. The wind changes, and pressure and temperature excursions from 2334 to about 0015 will be called *Event 2*.

From the sequence in which Event 1 arrived at the airport sensors, Bankstown, Lidcombe and ORS1, it can be deduced that the disturbance came from a south-westerly direction – consistent with the location of the thunderstorm centre. When possible disturbance centres are identified from the radar pictures, the best candidate appears to be a zone of high reflectivity that occurred around 2010, 110 km from the airport and on a bearing of 233° from it. This corresponds to the position of the storm centre at that time and is marked on Figure 2. Given the location of the disturbance, the speed of travel of Event 1 can be estimated by the time lag in the arrival of the wind change at different sensors and ORS1, assuming the front is circular with its centre at the disturbance origin. (Over the part of the Sydney basin in Figure 1 where this estimate is being made, a 110 km-radius front appears almost linear.) Choice of other possible disturbance centres results in only small variations (about 1°) in the lines of travel of the phenomenon to the various sites.

The change of the wind direction through due easterly at the start of the first undulation is used to define the arrival of the phenomenon. Using the disturbance source location posited above, the estimated travel speed in the 'east-airport region' (bounded by sensor 5, sensor 6 and ORS1) is 9.0 ± 1.0m s^{-1} or 32 ± 4km h^{-1}. The direction of travel in this region is on a heading of about 53° from north. Relative to the ambient wind in the 'east-airport region', the phenomenon travelled at about 16.5 ± 1.0m s^{-1}. It is likely that the phenomenon was travelling faster closer to its source, so the average speed over the entire run from the storm centre to the Sydney basin is probably higher than 9 m s^{-1}. Indeed, to get to the airport at 2135 from a postulated origin at 2010 this average speed would have to be 21-22 m s^{-1}. In any case, as noted in §3 below, it is unlikely that the same propagation mechanism prevailed over the entire run.

3 Gravity-wave calculations

a. A wave interpretation

In this section it is presumed that the observations at the airport can be explained as wave oscillations in the atmospheric boundary layer, rather than a gravity current of undular form. That is, the motion is considered to be essentially oscillatory (and, as a theoretical necessity in the following analysis, of 'small' amplitude), as opposed to a motion consisting of a density-driven outflow of mass.

Radiosonde measurements made at the airport at 0600 and 1500 show that there was a stably stratified layer in the form of a temperature inversion (Figure 6) which had persisted throughout the day. Internal waves could propagate within this layer, if the vertical wind profile were suitable. In the 'wave' interpretation of Event 1, the thunderstorm to the south-west of the airport generated a disturbance (probably a precipitation-generated downburst giving rise to an outflow of cold air) in the stratified layer that sent waves towards the airport, well before the storm itself moved into the airport area at 2230. The probable disturbance centre is in hilly country where the coastal inversion and wind profile would not be continuous (perhaps existing only in the valleys). So the disturbance probably travelled initially as a gravity current, generating an undular bore or a set of waves when it impacted the main inversion layer on entering the coastal Sydney basin.

The previous day's soundings had also shown an inversion. The inversion was therefore quite persistent; it had not been dissipated on either day, even at sounding times just after the day's maximum in solar heating. Unfortunately, a temperature sounding just before Event 1 (in the evening) was not made, however the persistence of the inversion indicated that it was strong enough to retain its form into the evening. It is assumed that the unstable layer is no longer present, because the solar heating creating it has gone and because the ground is known to have cooled: the 2130 dry-bulb temperature is about 4° cooler than the ground temperature at the sounding time (the dewpoint is a degree higher). The data from the sounding at 1500 has been adjusted to include the actual ground-level temperatures just before the phenomenon at 2130.

The observations in §2 indicate that the lower atmosphere was unsaturated and that there were no low clouds or precipitation present over the airport at the time of Event 1. The buoyancy (or Brunt-Väisälä) frequency is given by

$$N = \left(\frac{g}{\theta_v} \left(\frac{\mathrm{d}\theta_v}{\mathrm{d}z} \right) \right)^{\frac{1}{2}}, \tag{1}$$

where θ_v is the virtual potential temperature and z is height AGL. The moisture correction used to calculate θ_v was obtained from the same sounding that provided the dry-bulb temperature at 1500.

In Figure 6, the sounding temperature data has been plotted, along with a fitted curve. The original datapoints were from the radiosonde significant levels. For calculations to be described shortly, including the calculation of

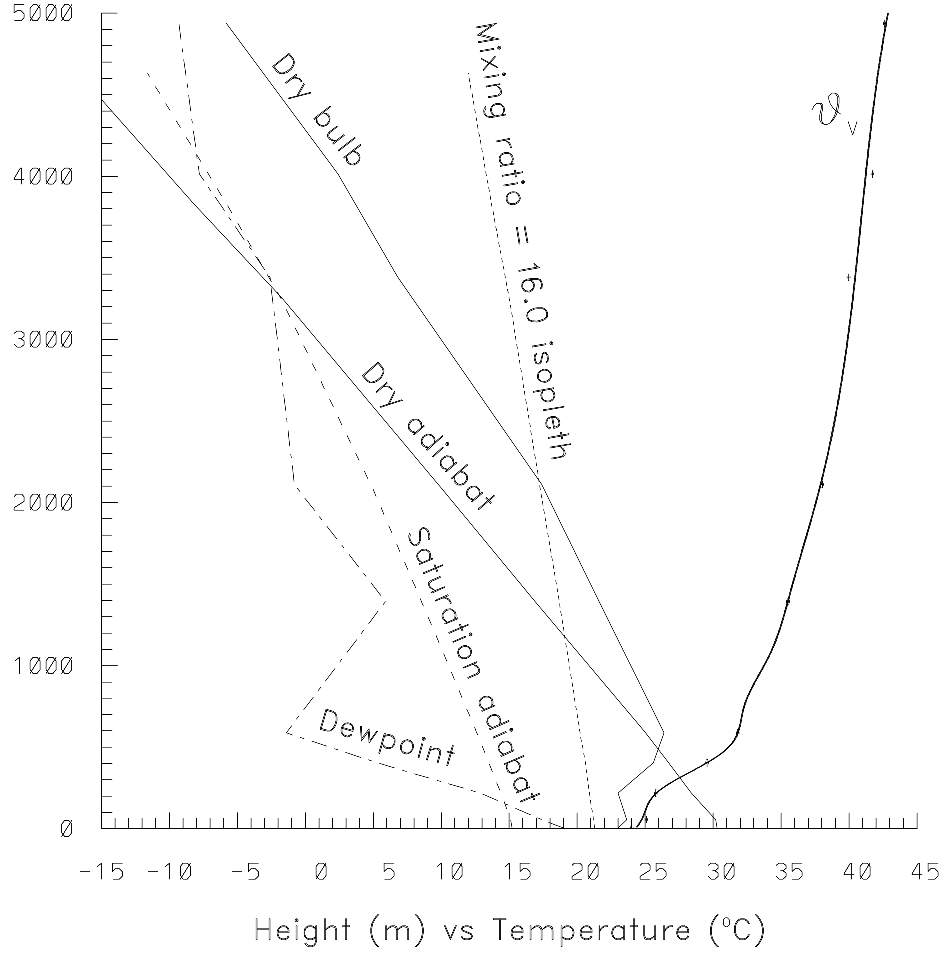

Figure 6: The radiosonde temperature profile of the lower atmosphere at 1500 on 27 December 1991. Points near the virtual potential temperature (θ_v) curve are the actual datapoints, to which the curve had been fitted by polynomials and functions of form $\exp(-az^2)\sin^2 bz$. The wet-bulb trace is reproduced without any fitting. The ground-level temperatures used are the ones measured at 2130; it is anticipated that the rest of the profile would not have been appreciably altered before 2130.

the Scorer parameter and vertical wavenumber profiles, the fitted curve was used in order to obtain a smooth result. However, the calculations were also made with linear lapse rates as a check. These results, to be detailed later, determined that the significant features of the profiles – their shape and zero-crossing altitudes – were not biased by the fitting process.

The undulations evident in Figure 3, viewed as wave oscillations, have a mean period of 14.5 minutes with a standard deviation of 1.5 minutes. This observation is of the period Doppler-shifted by the component of prevailing wind opposing propagation. Using the observed (Doppler-shifted) propagation speed of about 9 m s^{-1}, the horizontal wavelength of the waves becomes about 8 km.

Radar ranging measurements were made of an un-instrumented balloon released from the airport at 2100, providing a measurement of the wind profile about half an hour before the passage of the phenomenon. These are shown in Figure 7, along with a fitted curve.

b. Theory

The treatment below presumes that waves in the atmospheric boundary layer are trapped at some height. The trapped layer then provides a waveguide that channels the wave energy horizontally rather than permitting it to propagate upwards. This approach has often been used; good examples are the work of Noonan and Smith (1985), Doviak et al (1991) and Rottman and Einaudi (1993). The goal is therefore to determine if a trapping height exists for a small-amplitude sinusoidal wave moving horizontally with the observed speed of the disturbance.

1) LINEAR THEORY

The formulation below establishes the framework for a linear and weakly non-linear theory. Consider two-dimensional flow in a horizontally-homogeneous layer overlying the ground, which is stably stratified and subjected to a wind that varies with height. The two–dimensional momentum equations are

$$\rho^* \left(\frac{\partial u^*}{\partial t^*} + u^* \frac{\partial u^*}{\partial x^*} + w^* \frac{\partial u^*}{\partial z^*} \right) \quad = \quad -\frac{\partial p^*}{\partial x^*}, \tag{2}$$

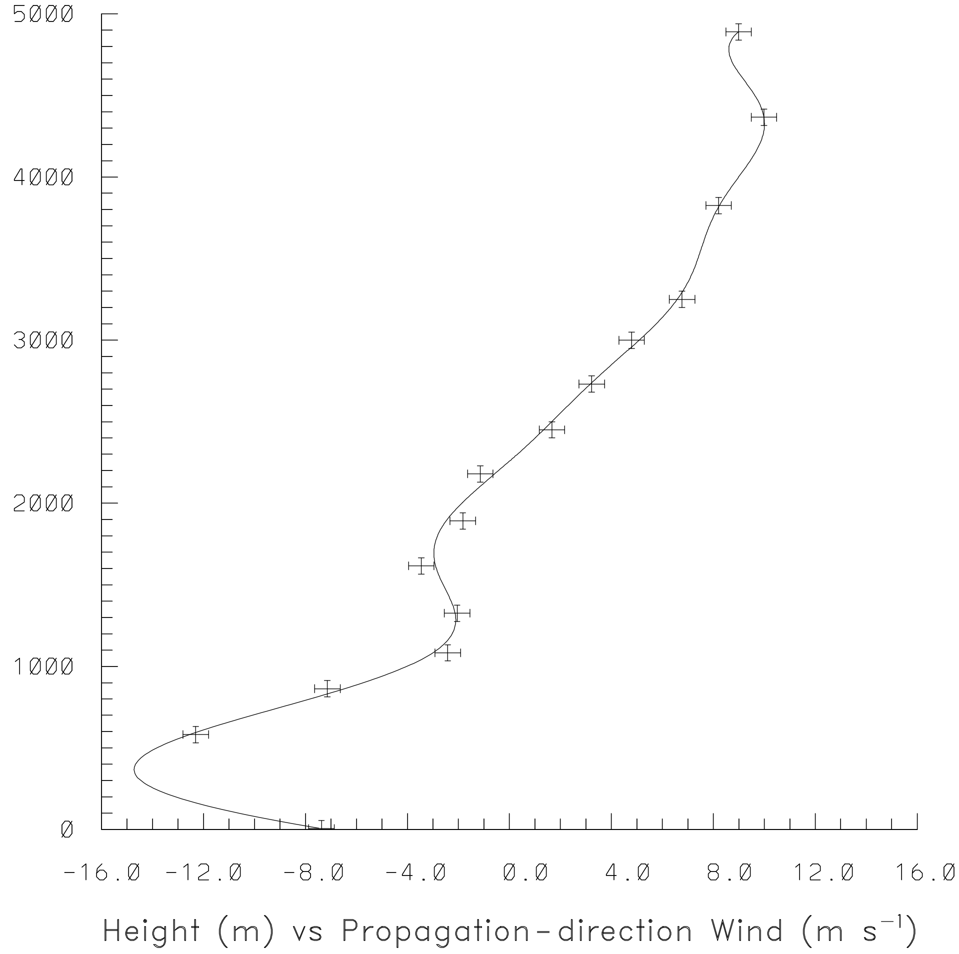

Figure 7: Radar wind profile from a piball sounding made at 2100, 27 December 1991. The curve is a fit to the datapoints shown using polynomial and sinusoidal functions. The component of the wind plotted is in the estimated direction of propagation of the phenomenon at the airport (on a heading of 53° from north).

$$\rho^* \left(\frac{\partial w^*}{\partial t^*} + u^* \frac{\partial w^*}{\partial x^*} + w^* \frac{\partial w^*}{\partial z^*} \right) = -\frac{\partial p^*}{\partial z^*} - g\tilde{\rho}^*, \tag{3}$$

where the asterisk indicates dimensional quantities. Here t^* is time, (u^*, w^*) are the horizontal and vertical components of velocity, x^* is in the direction of wave propagation, z^* is vertically upwards and p^* is pressure. The density is $\rho^* = \rho_s^* + \tilde{\rho}^*$, where ρ_s^* is the hydrostatic density and $\tilde{\rho}^*$ is the variation from this. The variation in density will be retained in the inertia terms so a Boussinesq approximation is not being made.

The incompressibility condition is expressed by

$$\frac{\partial \rho^*}{\partial t^*} + \mathbf{u}^* \cdot \nabla^* \rho^* = 0. \tag{4}$$

A scaling will be introduced that implicitly shifts the co-ordinate system into one moving with a phase speed c_0, and which makes the assumption that in this frame both components of velocity are small, $O(\varepsilon)$, as is the density variation. Now

$$(u^*, w^*) = N_0 L(\varepsilon u + U(z) - c_0, \varepsilon w), \tag{5}$$

$$t^* = N_0^{-1} t, \tag{6}$$

$$\rho^* = \rho_0(\rho_s + \varepsilon\tilde{\rho}), \tag{7}$$

where N_0 is a reference buoyancy frequency, L is a length scale characteristic of the motion and $U(z)$ is the height–dependent wind in the direction of wave propagation. The momentum equations can be combined by the introduction of a streamfunction, ψ, consistent with the incompressibility assumption,

$$\frac{\partial \psi}{\partial z} = u, \tag{8}$$

$$\frac{\partial \psi}{\partial x} = -w, \tag{9}$$

giving to leading order the linear expression

$$\begin{aligned} \frac{\partial \rho_s}{\partial z} \left(\frac{\partial^2 \psi}{\partial z \partial t} \right. &+ \left. (U - c_0) \frac{\partial^2 \psi}{\partial z \partial x} - \frac{\partial \psi}{\partial x} \frac{\partial U}{\partial z} \right) \\ &+ \rho_s \left[\frac{\partial}{\partial x} \left((U - c_0) \nabla^2 \psi - \psi \frac{\partial^2 U}{\partial z^2} \right) \right] = \frac{g}{N_0^2 L} \frac{\partial \tilde{\rho}}{\partial x}, \end{aligned} \tag{10}$$

while the incompressibility condition becomes

$$\frac{g}{N_0^2 L}\left(\frac{\partial \tilde{\rho}}{\partial t}+(U-c_0)\frac{\partial \tilde{\rho}}{\partial x}\right)=-\frac{\partial \psi}{\partial x}\rho_s N^2(z), \tag{11}$$

where the height–dependent dimensionless buoyancy frequency, $N^2(z)$, is given by

$$N^2(z)=-\frac{g}{N_0^2 L}\frac{1}{\rho_s}\frac{\partial \rho_s}{\partial z}, \tag{12}$$

or equivalently in terms of potential temperature θ by

$$N^2(z)=-\frac{g}{N_0^2 L}\frac{1}{\theta}\frac{\partial \theta}{\partial z}. \tag{13}$$

Looking for solutions that are steady in the frame of reference moving at c_0 and wave-like in x,

$$\psi = A_0 \mathrm{e}^{\mathrm{i}kx}\Phi(z), \tag{14}$$

where A_0 is a constant amplitude, k is the wavenumber and $\Phi(z)$ is the vertical structure of the streamfunction, allows (10) and (11) to be combined to give

$$(\rho_s \Phi')' + \left[\rho_s \frac{N^2}{(U-c_0)^2} - \rho_s \frac{U''}{U-c_0} - \frac{\rho_s' U'}{U-c_0} - \rho_s k^2\right]\Phi = 0, \tag{15}$$

where $' \equiv \dfrac{\partial}{\partial z}$.

Together with appropriate boundary conditions, (15) forms a Sturm–Liouville problem for the vertical eigenfunctions of atmospheric waves.

Note that if the Boussinesq approximation were used, the ρ_s' terms (with the exception of the ρ_s' in N^2) would be neglected, and (15) would reduce to

$$\Phi'' + (\ell^2(z) - k^2)\Phi = 0, \tag{16}$$

where $\ell^2(z) = \dfrac{N^2}{(U-c_0)^2} - \dfrac{U''}{U-c_0}$ is Scorer's parameter. If the long–wave limit, $k \to 0$, were used, (16) becomes the Taylor–Goldstein equation for long waves.

It is convenient to express (15) in terms of the streamline displacement η, which is related to ψ by the transformation

$$\eta = c_0^{-1}\psi, \tag{17}$$

so in the long wave limit (15) then becomes

$$\left(\rho_s \bar{c}_0^2 \phi'\right)' + \rho_s N^2 \phi = 0, \tag{18}$$

where the definition of $\bar{c}_0 = c_0 - U$ and $\phi = c_0^{-1}\Phi$ makes (18) identical to (2.37) in Rottman and Einandi (1993).

A third version of (15) is obtained using the transformation

$$W = \rho_s^{\frac{1}{2}} w, \tag{19}$$

so that (15) becomes

$$\varphi'' + \left[\frac{N^2}{(U-c_0)^2} - \frac{U''}{(U-c_0)} - \frac{1}{2}\left(\frac{\rho_s'}{\rho_s}\right)' - \left(\frac{1}{2}\frac{\rho_s'}{\rho_s}\right)^2 + \frac{U'\rho_s'}{\rho_s(U-c_0)} - k^2\right]\varphi = 0, \tag{20}$$

where $\varphi = -\rho_s^{\frac{1}{2}}\Phi$. This non-Boussinesq formulation has an advantage over (15) and (18) in that it presents the square of the vertical wavenumber m in the term in square brackets. Otherwise under the Boussinesq approximation m is given by

$$m^2 = \ell^2(z) - k^2, \tag{21}$$

If at some height m^2 becomes negative, (16) no longer admits wave solutions there and the ray paths must turn and reflect back at $m = 0$. Hence wave energy from a lower altitude would not be able propagate upwards through a region of negative m^2 and would reflect downwards; a waveguide would exist. The importance of the curvature in wind (the U'' terms in expressions for m^2) in creating a trapped layer is exemplified in the numerical experiments of Crook (1988). These show that trapping owing to the curvature is responsible for a large amplitude, rather than convergence caused by the opposing wind.

Where $U \simeq c_0$, $m \to \infty$ and there is a critical level where the vertical wavelength becomes extremely short. Again, wave energy cannot propagate up through this level, though in this case the energy may be lost to turbulence rather than reflected.

A plot of m^2 is shown in Figure 8. Here the observed propagation speed has been used for c_0. In this case the Boussinesq approximation is good; a plot of the term in square brackets in (20), which is non-Boussinesq, showed little difference.

It can be seen that m^2 becomes negative at a height of about 700 m, returns to positive at 1450 m and is just zero again at about 2300 m. A critical level is present at about 4100 m. When m^2 is calculated without any fitting of the temperature profile, the region of imaginary m is still from about 700 m to 1450 m and a minimum near zero at about 2300 m is also found (as is, of course, the critical layer). Only the 'bulge' in the m^2 profile from 2300 m to 3200 m appears to be a spurious result of the fitting process. The profile of m^2 in the bottom 500 m of the atmosphere is essentially dominated by the profile of the buoyancy frequency N that comes from the temperature profile; the wind curvature term in (16) has little influence there.

2) WEAKLY NONLINEAR THEORY

It is important to note that, as an alternative to the linear–wave assumption (14), scalings of x and t could be assumed that permit a balance between dispersion and nonlinearity. A description of the required matching criteria used in the formal derivation of the following expressions can be found in Rottman and Einaudi (1993), the notation of which is followed hereafter. Then, under the weakly nonlinear approximation

$$\psi = A(x,t)\Phi(z), \tag{22}$$

a Sturm–Liouville problem in the form of (15) is still obtained for the vertical eigenfunction Φ. The amplitude function A satisfies the Benjamin–Davis–Ono (BDO) equation,

$$\frac{\partial A}{\partial t} + c_0\frac{\partial A}{\partial x} + \alpha A\frac{\partial A}{\partial x} + \mu\frac{\partial^2}{\partial x^2}\left[\frac{1}{\pi}\int_{-\infty}^{\infty}\frac{A(\xi)}{x-\xi}d\xi\right] = 0, \tag{23}$$

appropriate to a weakly stratified upper layer, or the Korteweg–de Vries (KdV) equation,

$$\frac{\partial A}{\partial t} + c_0\frac{\partial A}{\partial x} + \alpha A\frac{\partial A}{\partial x} + \beta\frac{\partial^3 A}{\partial x^3} = 0, \tag{24}$$

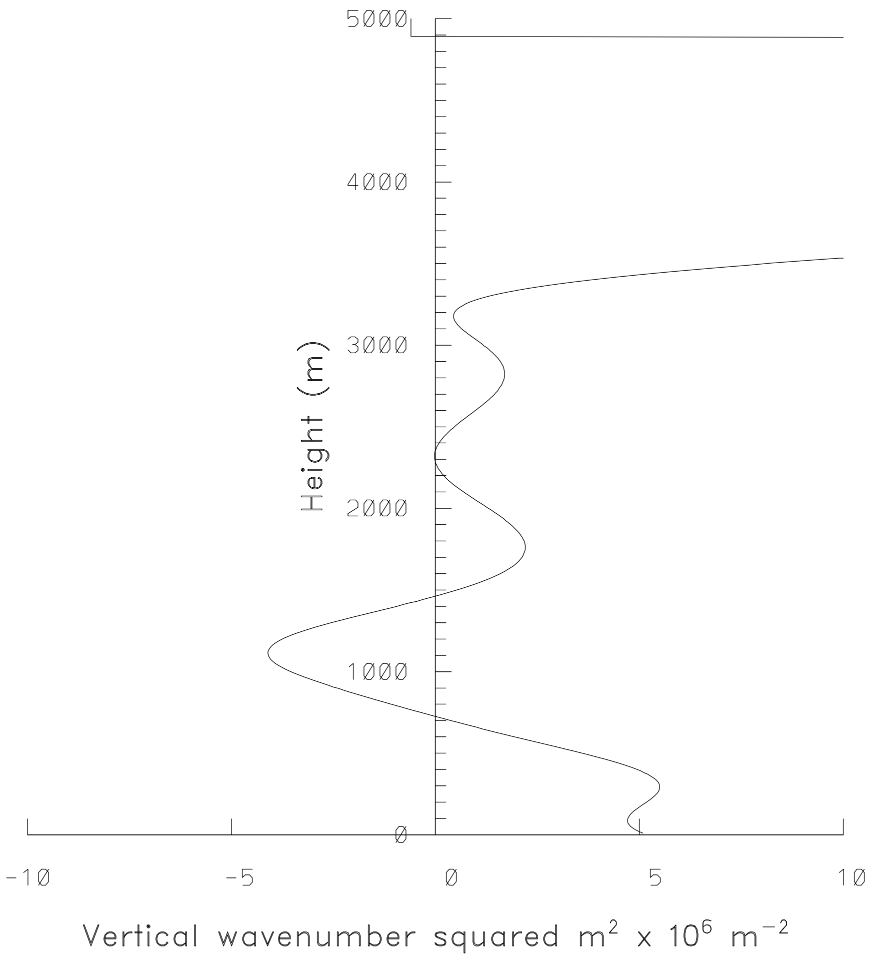

Figure 8: The vertical wavenumber m^2, using the observed propagation speed as the eigenvalue c_0.

if a 'rigid lid' tops the waveguide. In (23) and (24) the parameters α, β and μ are determined by the expressions

$$\alpha = I\int_0^D 3\rho_s\bar{c}_0^2(\phi')^3dz, \tag{25}$$

$$\beta = I\int_0^D \rho_s\bar{c}_0^2\phi^2dz, \tag{26}$$

$$\mu = I\left(\rho_s\bar{c}_0^2\phi^2\right)_{z=D}, \tag{27}$$

and

$$I = \left[\int_0^D 2\rho_s\bar{c}_0(\phi')^2dz\right]^{-1}, \tag{28}$$

in which D is the trapping height (the depth of the waveguide) and $\bar{c}_0$ and ϕ are determined by the solutions to the linear eigenvalue equation (18) which is subject to boundary conditions

$$\phi(0) = 0, \tag{29}$$

$$\phi'(D) = 0 \quad (\text{BDO}) \quad \text{or} \quad \phi(D) = 0 \quad (\text{KdV}). \tag{30}$$

The co-efficients α, β and μ are most compactly expressed in terms of the vertical structure eigenfunction for the streamline displacement ϕ. To calculate the weakly nonlinear correction c_1 to the linear phase speed c_0 it necessary to define the small parameter ε used the expansion which led to (25)-(27). Choose $\varepsilon = a/D$, where a is the maximum vertical streamline displacement. Then the weakly nonlinear phase speed is given by $c = c_0 + \varepsilon c_1$, where well-known solitary wave solutions (Benjamin 1967; Davis and Acrivos 1967) give

$$c_1 = \frac{1}{4}\alpha D, \tag{31}$$

the amplitude function $A(x)$ and the wave half-width parameter λ are given by

$$A(x) = \frac{a}{(x^2/\lambda^2)+1} \tag{32}$$

$$\text{and} \lambda^2 = \left(\frac{4\mu}{\alpha a}\right)^2, \tag{33}$$

and for the kDV equation they are given by

$$c_1 = \frac{1}{3}\alpha D, \tag{34}$$

$$A(x) = a\ \mathrm{sech}^2(x/\lambda) \tag{35}$$

$$\text{and}\lambda^2 = \frac{12\beta}{\alpha a}. \tag{36}$$

c. Estimations of wave propagation speeds and comparisons with data

An initial check can be made to see if the results are consistent with wave phenomena. This is done with linear plane-wave theory and by utilizing the velocity amplitude and pressure data. The polarization relation (Gill, 1982) relates the horizontal velocity component amplitude u of an internal wave to the perturbation pressure by

$$u = k\frac{p\prime}{\omega\rho_0}, \tag{37}$$

where k is the horizontal wavenumber, $p\prime$ is the amplitude of the perturbation pressure, ρ_0 is the unperturbed density and

$$\omega = \frac{kN}{(k^2+l^2)^{\frac{1}{2}}}. \tag{38}$$

For long waves, (37) reduces to

$$u = \frac{p\prime l}{N\rho_0}. \tag{39}$$

Although the maximum pressure rise during Event 1 is 3 mbar, an average value for the pressure amplitude $p\prime$ over the three observed undulations is 0.85 mbar. A height-average $\bar{u}$ of u over the first 700 m of the atmosphere gives an estimated amplitude of about 5 m s^{-1}. The amplitude of the observed undulations in velocity, as noted in §2, varies from about 4 to 7 m s^{-1}, so this estimate is reasonable. Noonan and Smith (1985) made estimates of the pressure rise using Bernoulli's equation for morning glories and obtained reasonable agreement in one case.

The formal way to obtain the theoretical value of the wave speed c_0 is to seek eigensolutions for (16) over $0 \leq z \leq D$. To do this, a numerical code was used to solve (15) for appropriate boundary conditions. As a check, solutions were also found using the equivalent formulations (18) and (20). The method employs the common 'shooting method' for solving eigenvalue problems based on ordinary differential equations. Given a trial eigenvalue, a Runge-Kutta routine solves the equation using the ground-level boundary condition $\phi(0) = 0$ as an initial condition. The discrepancy from the required boundary condition at the upper limit of the integration is used as the closeness-to-zero variable in a root-finding routine. This loops over the whole process until convergence is to the eigenvalue obtained or until the root finder fails, indicating that there is no solution for the boundary conditions chosen. Standard shooting-method packages are also available; one was used to check our code and confirmed its accuracy; however, the numerical conditions required by the package's method could not always be satisfied on the present problem, necessitating reliance on our code. Refer to Table 1 which summarizes the results for different choices of the trapping height D, and recall that the observed wave speed is 9.0 ± 1.0 m s^{-1} and estimated wavelength 8 km.

Realistic solutions could not be obtained using boundary conditions appropriate to the KdV equation. The best agreement is for boundary conditions appropriate to the BDO equation and a waveguide 2300 m deep. The corresponding eigenfunction remains smooth and well-behaved above 2300 m, decreasing until the critical layer is reached. There are difficulties, however, in finding a physical interpretation consistent with this result. This is discussed in the next section.

It can be seen that the above linear result alone, albeit of questionable interpretation, is adequate for agreement with the observation. For consistency with both the observation and the spirit of small-amplitude theory, the weakly nonlinear correction εc_1 should be small. The weakly nonlinear correction is calculated by using the observed maximum pressure rise to give the maximum displacement a. Rottman and Einaudi (1993) point out that this should be done consistently with the weakly nonlinear approximation. From Table 1, the result is acceptably small. However, a λ of 13.7 km is much too large; a wave half-width commensurate with the observations would be about 4 km. These two features of the nonlinear analysis – a lack of improvement over linear theory and an over-estimation of the wave half-widths by a factor

D (m)	c_0 (m s^{-1})	εc_1 (m s^{-1})	c (m s^{-1})	λ (km)
			(9.0 $\pm$ 1.0)	($\sim$ 4)
4000	15.8	0.2	16.0	27.1
2500	9.7	0.3	10.0	14.7
2300	8.6	0.3	8.9	13.7
2000	6.7	0.4	7.1	11.8
1500	2.6	0.6	3.2	3.1
$<$ 1500		No solution		

Table 1: Calculated values for the linear phase speed c_0, the nonlinear correction εc_1, the resulting overall phase speed c and the wave half-width λ as a function of the waveguide D, under boundary conditions appropriate to the BDO equation. Observed values are in brackets.

of two or three – were also found by Noonan and Smith (1985). Rottman and Einaudi were able to achieve good agreement on the same data by using a much greater amplitude of more than half the waveguide depth. They note that this is probably in excess of the bounds of weakly nonlinear theory.

4 Discussion

In the absence of vertical kinematic and thermodynamic data, we can only speculate on the true nature of the phenomenon. Nevertheless, it seems improbable that Event 1 was a pure gravity current. There is no consistent drop in temperature that would characterize the passage of a cold mass of air. The meteorological station continued to report clear air throughout the event, even though more frequent observations were made when its staff noticed the start of the first undular rise in pressure. Moreover, the wind record shows that the wind speed dropped to zero and slightly reversed during the undulations. In contrast, a gravity current head has a sustained feeder current near ground level that exceeds the propagation speed.

It is unlikely that any outflow air-mass associated with Event 1 ever arrived at the airport in a coherent form. The only significant change in temperature that might characterize the arrival of a mass of outflow air is the drop from 21.4 at 2356 to 18.2 at 0004, which is associated with Event 2. Since the wind due to Event 2 is easterly, Event 2 may have been a local outflow from the thunderstorm that was at its climax above the airport at the time.

The amplitude of observed velocity and pressure oscillations of Event 1 is consistent with a wave interpretation. It appears that a linear theory for waveguide modes in a sheared stratified atmosphere can give a good estimate of the propagation speed of the observed undulations. The need to define the top to the waveguide at an altitude much higher than an initial region of negative m^2 (an evanescent region) was also found by Rottman and Einaudi (1993). They stated that the evanescent region in their data was not deep enough to trap all the wave energy. This explanation may also be used here to justify a waveguide depth of 2300 m. However, there are two significant difficulties in interpreting this result. Firstly, although Figure 8 shows that the m^2 profile does osculate to zero at 2300 m, this is of limited credibility as a trapping mechanism, given that atmospheric changes in the 6.5 hours between the sounding and the wave may have removed this zero in the profile. Secondly, there is a considerable evanescent region between the ground and the postulated top of the waveguide, so plane-wave disturbances from the lower levels would not have been able to energize the whole waveguide in which a wave mode is supposed to be trapped. This means that the excitation of a wave mode by a ground-level gravity current, a likely wave-generating mechanism (Fulton et al 1990), cannot be used to explain this result. Instead, some less satisfactory and unspecified upper-level disturbance must be invoked. A fully nonlinear alternative will be discussed shortly.

There is evidence that Event 1 is a train of solitary waves. The first indication of this is the decreasing amplitude of the undulations, which suggests that a family of amplitude-ordered solitary waves was propagating over the airport. The solitary wave with the largest amplitude travels fastest, and hence is first, however, evidence of the waves separating as they propagate is inconclusive. There does not appear to be a significant difference in the timings between the wave crests at sensor 6, where the undulations arrived first, and the crests recorded at the airport. For sensors 1-6, the average time between the first and second crests was 15 minutes and the average time between the second and third crests was 14 minutes. There was no significant difference in these times at a 90% statistical confidence level. At Bankstown, the time between first and second crests was about 17 minutes and about 14 minutes separated the second and third crests. By the time the waves had reached ORS1 the equivalent times were both roughly 17 minutes. This may indicate a separation of the waves, but is not convincing evidence. Regarding the propagation speed, atmospheric solitary waves reported previously (Clarke et al 1981; Doviak and Ge 1984; Hasse and Smith 1984; Noonan and Smith 1985; Fulton et al 1990) typically travelled at 10-20 m s^{-1}, as did the undulations reported here.

The weakly nonlinear correction shows a wave half-width too large for the observation, which is an indication that the weakly nonlinear approximation may be invalid. Alternatively, a fully nonlinear disturbance may be trapped in the bottom 700 m of the atmosphere, permitting consistency with the scenario where the wave mode is forced by a ground-level outflow.

5 Conclusions

A disturbance in a stably stratified, sheared atmosphere over Sydney Airport was generated, probably by a nearby thunderstorm, on the evening of 27 December 1991. It is surmised that the disturbance caused a train of waves to propagate in a waveguide. In the few minutes taken to cross the airfield, this phenomenon resulted in a 20 knot (10 m s^{-1}) wind shear across the ends of runway 16/34; this local low-level wind shear marginally exceeded the US Low-Level Wind Shear Alert System alarm threshold and may therefore be considered a hazard to aircraft.

There is evidence of amplitude ordering in the present observations, an indicator of solitary waves. Good agreement was found on the propagation speed of the phenomenon, using linear theory, but the weakly nonlinear analysis over-estimates the wave-half width. Further problems in the interpretation of this small-amplitude (linear and weakly nonlinear) result are the weakness of the trapping at 2300 m and the lack of a mechanism for forcing a mode in a waveguide of this depth. Similiar problems have been noted by others (Noonan and Smith 1985; Doviak et al 1991; Rottman and Einaudi 1993) in the analysis of apparently similar phenomena by small-amplitude theory. A more physically viable interpretation of the phenomenon would describe it as a family of fully nonlinear solitary waves originating from the breakdown of a thunderstorm outflow current, and trapped in the bottom

700 m of the atmosphere. This is exemplified by the experiments described in chapter 13 of Simpson (1987) and was suggested also by the observations of Fulton et al (1990). If this was the case, the oscillations may not have been pure 'waves'; they may have contained trapped outflow air.

Finally, it is worth noting that there exist conceptual and analytic tools based on wave mechanics that are useful for describing solitary waves (e.g. Benjamin 1967), and tools based on hydraulics used to treat gravity currents (e.g. Benjamin 1968). These models have separate theoretical bases that do not overlap. However, nature can provide us with a hybrid: a solitary wave may encapsulate some cold outflow air (Doviak and Ge 1984), and thus, like a current, transport mass as a first-order effect; alternatively, the head of a gravity current may detach and travel alone, like a solitary wave (Simpson 1987). There seems to be a continuum in the morphologies of the observed phenomena that is not yet mirrored by a general theory. The true physics of the present observations may lie between idealized concepts.

Acknowledgements

We have benefitted from discussions with a number of fluid dynamicists and meteorologists, notably Dr. Jim Rottman, formerly of NASA Goddard Space Flight Centre, who kindly used his own program to independently analyse some of our data, and Ken Batt and Philip King of the Australian Bureau of Meteorology, Severe Weather Group, Sydney. Advice from Dr. Roger Smith and an anonymous reviewer resulted in a much improved version of this paper. We are grateful to Greg Nippard of UNSW who implemented the data links from the airport and devised the data pre-processing scheme, to the Australian Civil Aviation Authority for the provision of the data from their instruments and to Peter Tate of the Sydney Water Board for the data from ORS1. The sounding, Bankstown anemometer and radar data were provided by the Bureau of Meteorology. Anemometer data from Lidcombe was provided by the New South Wales Environment Protection Authority. This work was supported by the Australian Research Council (grant A89030563).

References

Balachandran, N. K., 1980: Gravity waves from thunderstorms. *Mon. Wea. Rev.* **108**, 804-816.

Benjamin, T. B. 1967: Internal waves of permanent form in fluids of great depth. *J. Fluid Mech.* **29**, 559-592.

——, 1968: Gravity currents and related phenomena. *J. Fluid Mech.* **31**, 209-248.

Christie, D. R. 1992: The morning glory of the Gulf of Carpentaria: a paradigm for non-linear waves in the lower atmosphere. *Aust. Met. Mag.* **41**, 21-60.

Clarke, R. H., Smith, R. K., and Reid, R. K., 1981: The Morning Glory of the Gulf of Carpentaria: An atmospheric undular bore. *Mon. Wea. Rev.* **109**, 1726-1750.

Crook, N. A., 1988: Trapping of low-level internal gravity waves. *J. Atmos. Sci.* **45**, *nȯ 10, 1533-1541.*

Davis, R. E., and Acrivos, A., 1967: Solitary internal waves in deep water. *J. Fluid Mech.* **29**, 593-607.

Doviak, R. J., and Ge, R., 1984: An atmospheric solitary gust observed with a Doppler radar, a tall tower and a surface network. *J. Atmos. Sci.* **41**, 2259-2573.

——, Chen, S. S., and Christie, D. R., 1991: A thunderstorm-generated solitary wave observation compared with theory for nonlinear waves in a sheared atmosphere. *J. Atmos. Sci.* **48**, 87-111.

Fujita, T. T., and Carcena, F., 1977: An analysis of three weather-related aircraft accidents. *Bull. Am. Met. Soc.* **58**, 11, 1164-1181.

Fulton, R., Zrnić, D. S., and Doviak, R. J., 1990: Initiation of a solitary wave family in the demise of a nocturnal thunderstorm density current. *Mon. Wea. Rev.* **47**, 319-337.

Gill, A. E., 1982: *Atmosphere-Ocean Dynamics.* Academic Press, London, 662pp.

Gossard, E. E., and Hooke, W. H., 1975: *Waves in the atmosphere.* Elsevier, Amsterdam, 456pp.

Hasse, S. P., and Smith, R. K., 1984: Morning glory wave clouds in Oklahoma: A case study. *Mon. Wea. Rev.* **112**, 2078-2089.

Lee, W.-C., Carbone, R. E., and Wakimoto, R. M., 1992a: The evolution and structure of a "Bow-echo-microburst" event. Part I: The Microburst.

Mon. Wea. Rev. **120**, pp 2188-2210.
——, Wakimoto, R. M., and Carbone, R. E., 1992b: The evolution and structure of a "Bow-Echo-Microburst" event. Part II: The Bow Echo. *Mon. Wea. Rev.* **120**, pp 2211-2225.
Mahoney, W. P. III, and Elmore, K. L., 1991: The evolution and fine-scale structure of a microburst-producing cell. *Mon. Wea. Rev.* **119**, pp 176-192.
Noh, Y., Fernando, H.J.S., and Ching, C.Y., 1992: Flows induced by the impingement of a two-dimensional thermal on a density interface. *J. Physical Oceanography* **22**, 1207-1220.
Noonan, J. A., and Smith, R. K., 1985: Linear and weakly nonlinear internal wave theories applied to "Morning Glory" waves. *Geophys. Astrophys. Fluid Dyn.,* **33**, *123-143.*
Physick, W., 1986: Observations of a solitary wave train at Melbourne, Australia. *Aust. Met. Mag.* **34**, pp 163-172.
Rottman, J. W., and Simpson, J. E., 1989: The formation of internal bores in the atmosphere: a laboratory model. *Quarterly J. Royal Meteorological Soc.* **115**, 941-963.
——, Einaudi, F., 1993: Solitary waves in the atmosphere. *J. Atmos. Sci.* **50**, *nȯ 14, 2116-2136.*
Simpson, J. E., 1987: *Gravity currents: In the environment and the laboratory.* Ellis Horwood Limited (Wiley), 244 pp.
Shreffler, J. H., and Binkowski, F. S., 1981: Observations of pressure jump lines in the Midwest, 10-12 August 1976. *Mon. Wea. Rev.* **109**, 1713-1725.
Smith, R. K., 1986: Evening glory wave-cloud lines in northwestern Australia. *Aust. Met. Mag.* **34**, 27-33.